Sci. Technol. Adv. Mater. **11** (2010) 043001 (10pp) doi:10.1088/1468-6996/11/4/043001

TOPICAL REVIEW

Low-energy cathodoluminescence microscopy for the characterization of nanostructures

Benjamin Dierre[1,2], Xiaoli Yuan[1] and Takashi Sekiguchi[1,2]

[1] Advanced Electronic Materials Center, National Institute for Materials Science (NIMS), Tsukuba 305-0044, Japan
[2] Graduate School of Pure and Applied Sciences, University of Tsukuba, Tsukuba 305-0003, Japan

E-mail: sekiguchi.takashi@nims.go.jp

Received 24 November 2009
Accepted for publication 4 August 2010
Published 10 September 2010
Online at stacks.iop.org/STAM/11/043001

Abstract
Spatially and spectrally resolved low-energy cathodoluminescence (CL) microscopy was applied to the characterization of nanostructures. CL has the advantage of revealing not only the presence of luminescence centers but also their spatial distribution. The use of electrons as an excitation source allows a direct comparison with other electron-beam techniques. Thus, CL is a powerful method to correlate luminescence with the sample structure and to clarify the origin of the luminescence. However, caution is needed in the quantitative analysis of CL measurements. In this review, the advantages of cathodoluminescence for qualitative analysis and disadvantages for quantitative analysis are presented on the example of nanostructures.

Keywords: cathodoluminescence, nanostructures, wide band-gap semiconductors, rare-earth, phosphors, electron beam

1. Introduction

Optical characterization of nanostructures is usually performed by statistically averaging their ensemble. However, this approach is imprecise and sometimes misleading due to the possible coexistence of materials with different optical properties. With the development of low-dimensional optoelectronic materials, the investigation of local variations of luminescence is gaining importance [1, 2]. The low-energy cathodoluminescence (CL) technique has decisive advantages for this purpose. It allows characterization of individual nanostructures that can be used to evaluate materials for industrial applications, such as field emission displays. With CL, one can also map the luminescence distribution both laterally and along the sample depth that can provide precious information on the growth mechanisms. Finally, the combination of CL with other electron beam (e-beam) techniques allows to determine the origin of the luminescence.

CL is the emission of light from a material under e-beam irradiation [3, 4]. Compared with light, electron excitation is rather strong. The incident electrons generate a high density of electron–hole (e–h) pairs due to inelastic scattering—it is commonly accepted that an incident electron of energy E can generate $\sim E/3\mathrm{E_g}$ pairs [3, 4]. Those e–h pairs can recombine and emit photons. The energy of these photons depends on the energy difference between the electrons and holes, which is related to the bandgap E_g or to the energy levels of the impurities and defects. Consequently, CL can reveal most of the luminescence processes in the materials. Especially, the electron beam can excite high energy levels allowing to characterize deep ultraviolet (UV) emission from wide-bandgap materials, such as BN, which is very difficult to study with light-induced luminescence. Development of the electron microscopes improved control of the size and the position of the electron beam, allowing to acquire luminescence from nanoscale regions. By changing

 © 2010 National Institute for Materials Science Printed in the UK

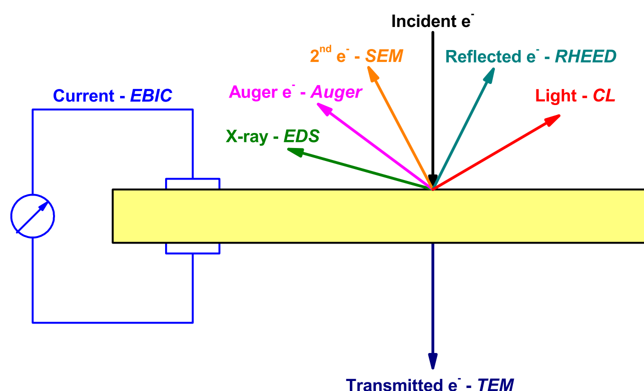

Figure 1. Schematic illustration of the signals generated by the electron irradiation of a non-metallic solid.

the energy of the incident electrons, it is possible to excite the material at different depths: the surface can be excited by low energy and deeper regions by higher energy electrons [5]. In this way, CL allows a lateral and depth resolved analysis of the distribution of luminescence centers present in the material. It should be noted that, although the CL generation volume is mainly related to the electron penetration range, it is also affected by the minority carrier diffusion, because light is generated not where the e–h pairs are generated, but where they recombine [6]. However, in semiconductor nanostructures, such diffusion is limited by the quantum confinement [7] and surface effects [8]. Finally, as illustrated in figure 1, the interaction of incident electrons with the material can generate various signals, which provide different information on the materials. Beside the optical properties from CL, structural information can be obtained from reflected (reflection high-energy electron diffraction, RHEED) and transmitted electrons (transmission electron microscopy, TEM), surface morphology from secondary electrons (scanning electron microscopy, SEM), chemical structure from Auger electrons (Auger electron spectroscopy) and x-rays (energy-dispersive x-ray spectroscopy, EDS) and electrical properties from the current induced due to the separation of generated e–h pairs (electron-beam induced current, EBIC). The combination of these techniques with CL results in a better understanding of the origin of the luminescence.

In summary, the advantages of CL for the characterization of the nanostructures are:

- Local excitation, allowing to map the lateral and depth distribution of the luminescence centers.
- Combination with other electron-based techniques, allowing to correlate optical, structural, chemical and electrical properties.
- Strong excitation, allowing to excite emission from deep UV to infrared (IR) spectral range.

In this review, we highlight the role of low-energy CL technique in the analysis of optical materials. The lateral and depth distribution, the combination with other electron-based techniques and the strong excitation are illustrated on example of nanostructures. Additionally, we show that caution must be exercised in a quantitative analysis of CL.

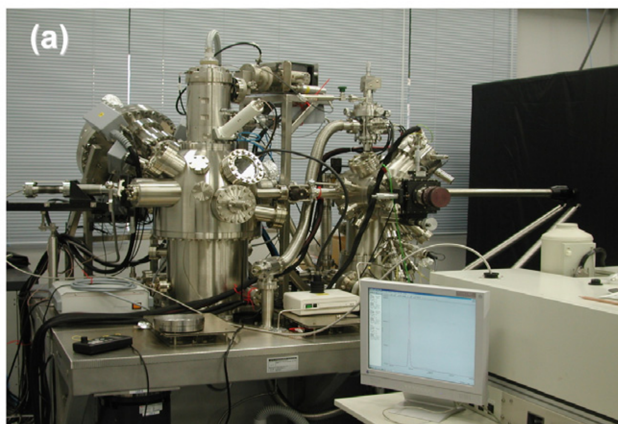

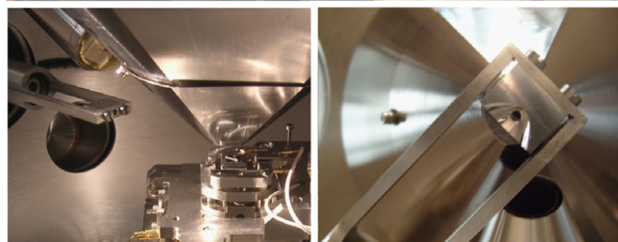

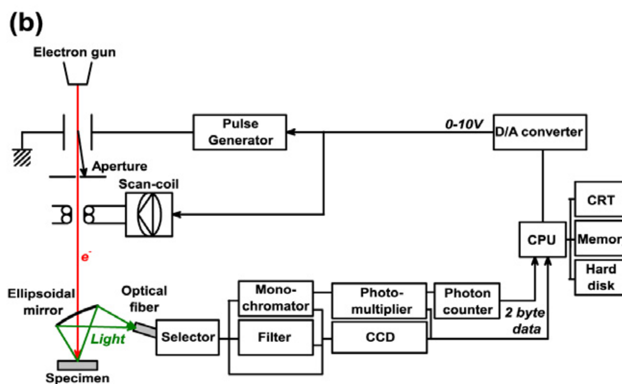

Figure 2. Photographs of the UHV-SEM CL system and the ellipsoidal mirror (a) and the block diagram of the CL system (b).

2. Experimental details

2.1. Cathodoluminescence system

CL measurements were performed with an SEM-based setup, which consists of a light collector, detection system and computer controller, as illustrated in figure 2. The electron source is a Schottky-type field emission electron gun (Omicron, Germany), allowing a beam diameter of the order of tens of nanometers. The electron energy can be varied from 1.5 to 25 kV. To reduce the surface contamination, we adopted an ultra-high vacuum system (less than 2×10^{-10} mbar).

The light-collection system consists of an ellipsoidal mirror of low magnification and an optical fiber. The ellipsoidal mirror is designed to realize both high and uniform collection efficiency. One focal point of the ellipsoid is set at the specimen position and another at the entrance edge of the optical fiber. Thus, the CL emission is focused on the entrance edge of the optical fiber and guided into a triple-grating monochromator (Jobin-Yvon Triax320). In spectral measurements, the dispersed light is detected by a

charge-coupled device with 2048 channels (CCD, Jobin-Yvon Spectrum One). Parallel detection of the spectrum with the CCD significantly reduces the acquisition time compared with the serial detection using a photomultiplier. One- or two-dimensional spectral mapping is also possible with this system. For imaging, monochromatic light is guided to the photomultiplier (Hamamatsu R943-02 or R3310-02). A photon counting system is adopted to record light emitted from each pixel point. The spectral resolution is determined by the grating and the slit width and is typically 0.2 nm.

2.2. Samples

The studied samples were rare-earth doped oxynitride phosphors (Ca and Yb codoped α-SiAlON and Eu-doped AlN) synthesized by gas-pressure sintering [9–14], Zn_2SiO_4 nanotubes obtained by reacting ZnO nanowires with SiO_2 [15], $ZnGa_2O_4$ nanowires grown by chemical vapor deposition (CVD) [16] and different types of ZnO materials. The latter included nanotubes (grown by metal organic chemical vapor deposition, MOCVD) [17, 18], nanoparticles (vapor method) [19], nanoflowers (hydrothermal method) [20], tetrapods composed of nanorods (catalyst-free vapor-solid growth) [21], polycrystals [22] and single crystals (hydrothermal synthesis) [23].

3. Advantages of CL

3.1. Local excitation

3.1.1 Spatial distribution. The main advantage of CL microscopy is local excitation, which makes it especially suitable for optical characterization of nanostructures. Precise control of the size and position of the e-beam in the electron microscope allows to acquire a CL spectrum from a nanoscale region. Moreover, by scanning the material, it is possible to obtain high-resolution CL images of the luminescence centers [15, 21, 24–29]. Such information is important for nanomaterials as it can provide information about the growth mechanisms.

We have investigated the luminescence properties of Zn_2SiO_4 nanotubes on Si substrate. The tubes were synthesized from ZnO nanowires reacting with SiO_2 [15]. Figure 3 shows cross-sectional SEM images of ZnO nanowires (a) and Zn_2SiO_4 nanotubes (b) and their averaged CL spectra (c) at 5 kV and 1.0 nA. The SEM images reveal that the Zn_2SiO_4 nanotubes are thicker than the ZnO nanowires due to the formation of a SiO_2 coating [15]. Both the ZnO nanowires and Zn_2SiO_4 nanotubes lie on a buffer layer. The CL spectrum of the ZnO nanowires consists of excitonic emission at 380 nm and a broad band at 550 nm related to defects and/or impurities in ZnO [30, 31]. The CL spectrum of the Zn_2SiO_4 nanotubes, in addition to these two peaks at 380 and 550 nm, has two new bands at 310 and 440 nm. The 310 nm emission is attributed to defects in Zn_2SiO_4 [32] and the 440 nm peak to defects in SiO_2 [33].

The presence of the peak at 380 nm (excitonic emission of ZnO) from the Zn_2SiO_4 nanotubes sample indicates that the ZnO nanowires are only partly reacted with SiO_2 and

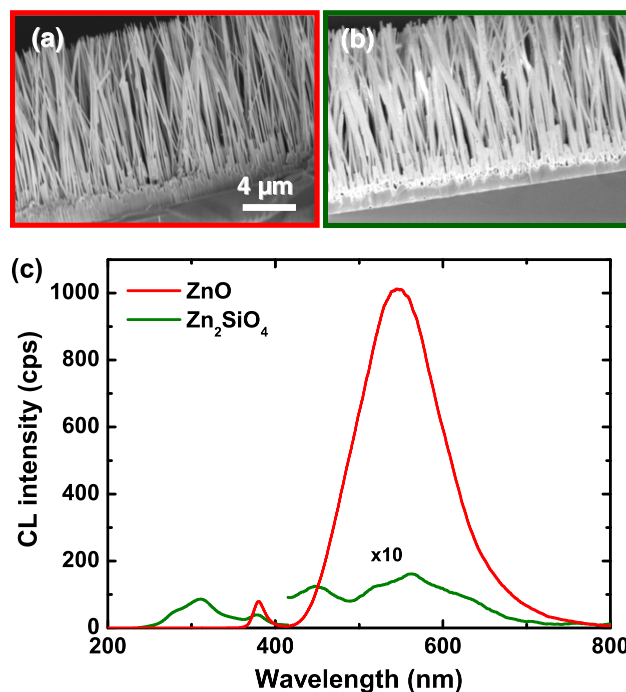

Figure 3. Cross-sectional SEM images of ZnO nanowires (a) and Zn_2SiO_4 nanotubes (b), and their CL spectra (c) at 5 kV and 1.0 nA.

some ZnO still remains. To test this hypothesis we mapped the CL distribution of the 310 and 380 nm emission. Figure 4 shows the SEM images of Zn_2SiO_4 nanotubes (a) and the corresponding CL images recorded at 310 nm (b) and 380 nm (c) with the e-beam voltage of 5 kV and 1.0 nA current. The 310 nm emission (defects of Zn_2SiO_4) is produced by the Zn_2SiO_4 nanotubes, whereas the 380 nm light (excitonic emission of ZnO) originates from the buffer layer. Moreover, the interface between the Si substrate and the buffer layer (indicated by the white arrow) has a clear 310 nm emission, suggesting that this interface consists of Zn_2SiO_4. To clarify this result, CL spectra were taken from the buffet layer and the nanotubes. The CL spectrum from the buffer (point 1) consists of a sharp and strong peak at 380 nm, and a small peak at 550 nm. On the nanotubes (points 2 and 3), the 380 nm peak disappears, while the 310 nm emission emerges. These results demonstrate that the original ZnO nanowires have reacted with SiO_2 to form Zn_2SiO_4 nanotubes, but the buffer layer is still ZnO.

The 310 nm emission (defects of Zn_2SiO_4) is not uniformly distributed along the Zn_2SiO_4 nanotubes (figure 4(b)). To reveal this inhomogeneity, a low packing density sample was made by removing Zn_2SiO_4 nanotubes from the Si substrate and depositing them on a TEM grid. Figure 5 shows the CL image of 310 nm emission from a region where Zn_2SiO_4 nanotubes have low density. CL from some tubes is rather uniform, but it shows bright dots along other tubes. Possibly, the uniform nanotubes consist of Zn_2SiO_4 nanotubes coated with SiO_2, and the non-uniform ones are Zn_2SiO_4 nanoparticles encapsulated in SiO_2 nanotubes. The ZnO nanowires may react with SiO_2 by different mechanisms, such as Rayleigh instability and

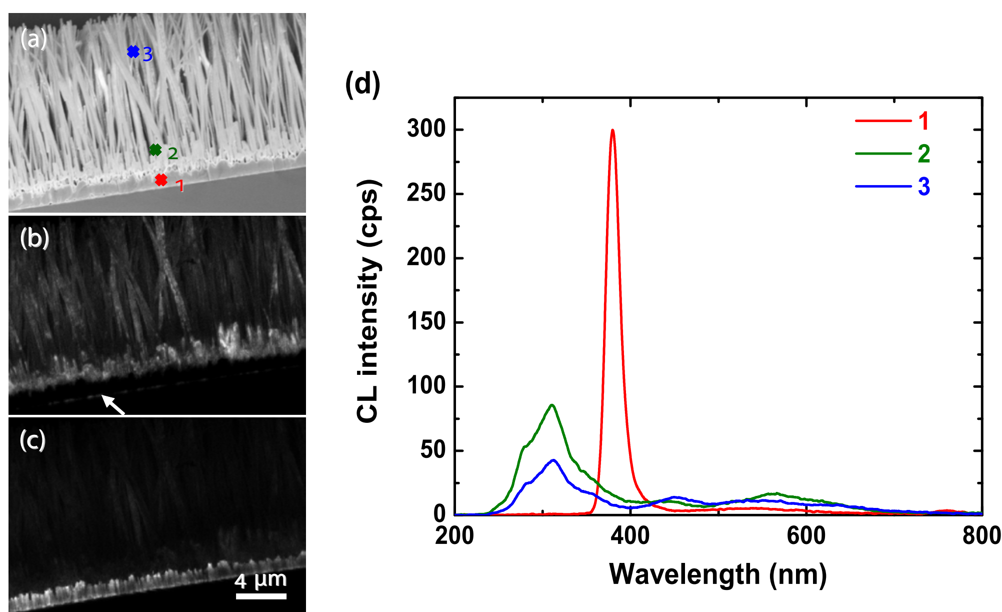

Figure 4. SEM images of Zn_2SiO_4 nanotubes (a) and the corresponding CL images of 310 nm (b) and 380 nm (c) emission generated at 5 kV and 1.0 nA. Panel (d) presents CL spectra taken at 5 kV and 1.0 nA from the buffer layer and the nanotubes at locations indicated in (a).

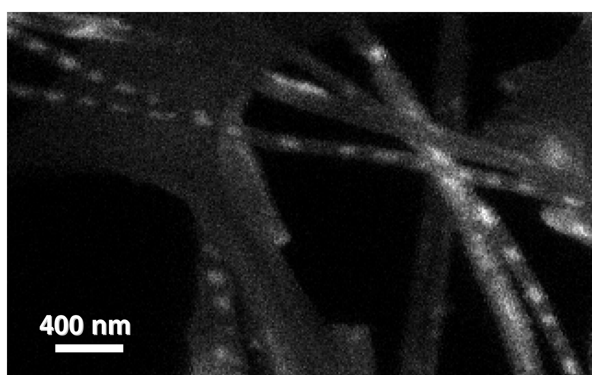

Figure 5. CL image of 310 nm emission from a low packing density Zn_2SiO_4 nanotubes, which were removed from the Si substrate and deposited on a TEM grid.

the Kirkendall solid-state reaction, which may result in the different tube structures [15].

3.1.2 Depth distribution. Not only the lateral but also the depth distribution of luminescence is important for the characterization of nanostructures. For instance, some nanostructures may be covered with oxide or other layers. There may also be some concentration gradient of defects, such as vacancies or impurities between the surface and the core of the nanostructures. By changing the electron energy, it is possible to vary the penetration depth of the incident electrons and excite the luminescence centers at different depth [34–37].

We have investigated the depth distribution of luminescence from $ZnGa_2O_4$ nanorods [16]. Figure 6 shows the SEM image of the nanorods (a) and the CL spectra (b) taken by varying the incident electron energy from 1.5 to 5 kV. For comparison, the CL spectra were normalized by the intensity at 360 nm. The luminescence consists of three peaks

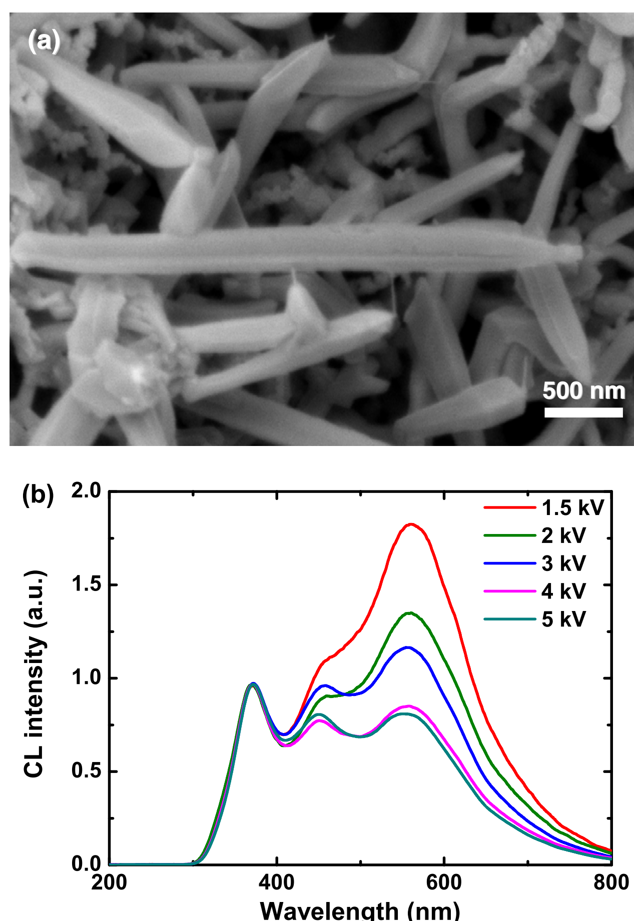

Figure 6. SEM image of $ZnGa_2O_4$ nanorods (a) and CL spectra (b) taken by varying the incident electron energy from 1.5 to 5 kV.

at 360, 450 and 550 nm, which are attributed to different defects in $ZnGa_2O_4$ [38–40]. At 1.5 kV, the 450 and 550 nm bands are stronger than that at 360 nm. When the electron

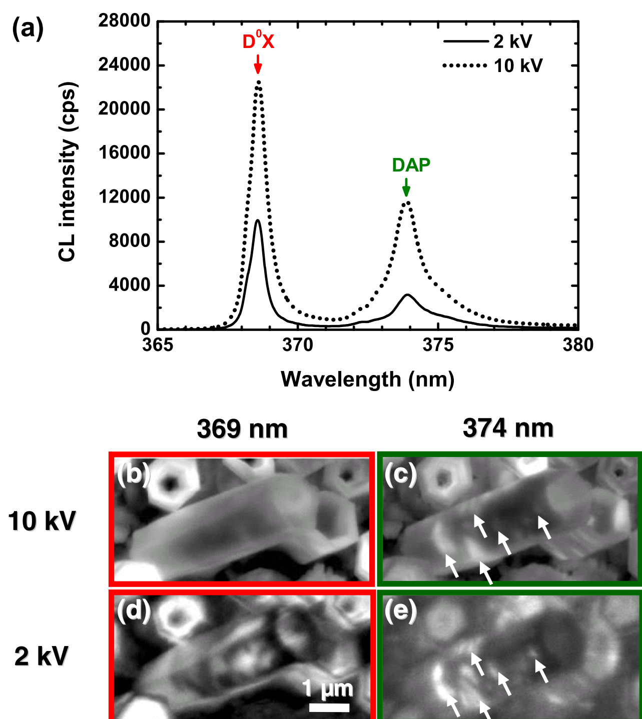

Figure 7. CL spectra of a tilted ZnO nanotube recorded at 10 kV/0.8 nA and 2 keV/0.2 nA at 10 K (a). CL images of 369 nm (b, d) and 374 nm (c, e) emissions for a tilted ZnO nanotube at 10 and 2 kV, respectively.

energy is raised to 5 kV, the 360 nm peak increases more than those of 450 and 550 nm and becomes dominant. The results suggest inhomogeneous defect distribution in the core and the surface regions.

By comparing the CL images taken at different accelerating voltage, it is possible to deduce the lateral and depth distribution of the luminescence centers. We have analyzed the luminescence from shallow levels of ZnO nanotubes grown on sapphire [18]. Figure 7(a) shows the CL spectra of a tilted ZnO nanotube recorded at 10 kV/0.8 nA and 2 kV/0.2 nA at temperature of 10 K. The excitation depth of the 2 kV electrons (penetration depth ∼50 nm) [5] allows revealing the thin walls of the tilted tubes, which have a thickness of about 150 nm. Electrons with the energy of 10 kV stop at the depth of ∼740 nm [5] and thus penetrate through the nanotubes; their CL signals are averaged over the nanotube thickness. The spectra consist of two peaks at 369 and 374 nm which are attributed to neutral donor excitonic emission (D^0X) and donor–acceptor pairs (DAP) transitions, respectively [41, 42]. We can assume that the intensities of the 369 nm (D^0X) and 374 nm (DAP) signals reflect the concentrations of donors and acceptors, respectively, at least for small defect concentrations. The CL images were taken for the 369 nm (b, d) and 374 nm (c, e) emissions in a tilted ZnO nanotube at 10 and 2 kV, respectively. For the D^0X (369 nm) luminescence, the 10 kV and 2 kV CL images are obviously different. Whereas the 10 kV distribution is relatively uniform, the 2 kV image clearly shows some patches along the nanotubes. On the contrary, the 10 kV and 2 kV CL images are rather similar for the DAP (374 nm) luminescence. The DAP luminescence is localized on some patches along the nanotubes, as indicated by the white arrows. The thus revealed inhomogeneous distribution of the donors and acceptors can be related to the unstable growth conditions and contaminations from the substrate and growth chamber.

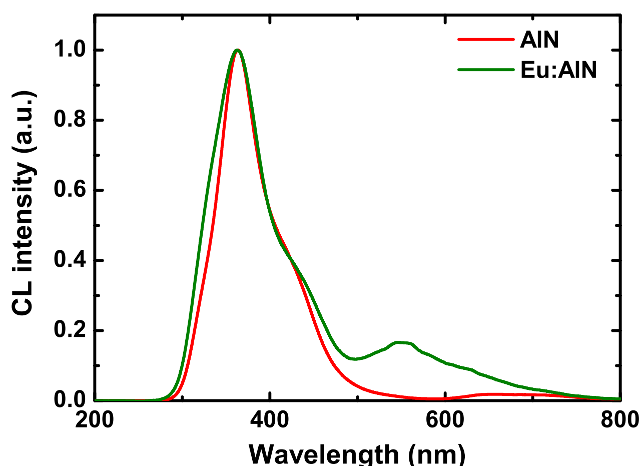

Figure 8. Normalized CL spectra for undoped AlN and AlN doped with 0.2% Eu.

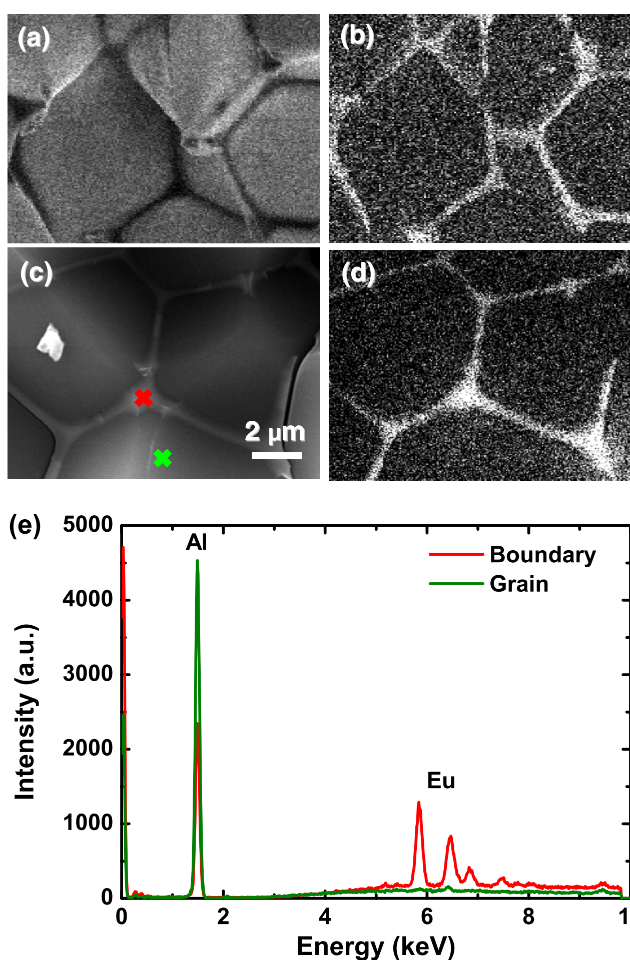

Figure 9. CL images of 360 nm (a) and 550 nm (b) emission of AlN:Eu. SEM image (c) and EDS image (d) of Eu distribution. Panel (e) shows EDS spectra taken from the grain and the grain boundary, as indicated in (c).

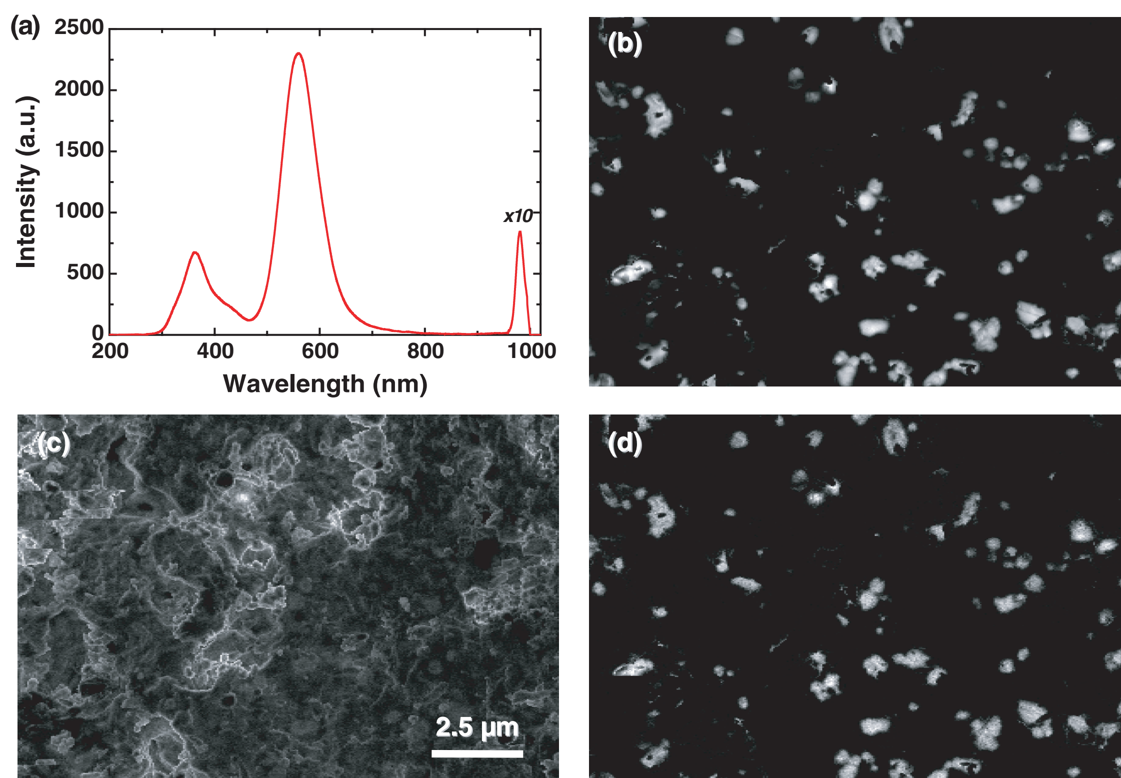

Figure 10. CL spectrum (5 kV) of Ca- and Yb-doped α-SiAlON (a). CL images of 360 nm (b), 557 nm (c) and 980 nm (d) emission.

3.2. Comparison with other e-beam techniques

Although luminescence and its distribution can be characterized with CL, this technique does not always supply enough information about the nature of the luminescence centers. In such cases, it is necessary to combine it with other techniques. Since the incident electrons can generate other signals beside CL, it is possible to correlate the light emission with electrical, chemical and structural properties. The correlation of CL with high-resolution TEM (HRTEM) and EBIC has been used to characterize defects, such as dislocations or stacking faults [43–47]. As for the variation of concentration/composition, the combination of CL with TEM, EDS or Auger spectroscopy can result in a better understanding of the origin of the luminescence [48, 49]. Here, we illustrate this aspect by the analysis of europium doping of AlN using the combination of CL and EDS [14].

Figure 8 shows the normalized CL spectra of undoped AlN and AlN:Eu (AlN doped with 0.2% Eu). The CL spectrum of undoped AlN shows a peak at 360 nm which is attributed to defects [50]. The CL spectrum of AlN:Eu consists of a strong peak at 360 nm and a weak band at 550 nm. Because the 550 nm peak appears with Eu doping, it would be reasonable to assign it to Eu^{2+} in AlN, as it was done by Hara *et al* [51]. However, this is not correct. Figures 9(a) and (b) show the CL images of 360 and 550 nm emissions in AlN:Eu, respectively. Whereas the 360 nm emission (defects in AlN) is almost uniform, the 550 nm band is restricted to the grain boundaries and therefore is hardly due to Eu^{2+} in AlN. SEM–EDS measurements were performed to confirm this result and clarify the origin of this emission. Figures 9(c) and (d) show the SEM image and the corresponding EDS image of the Eu distribution. Similar to the 550 nm CL signal, europium is concentrated at the grain boundaries. EDS spectra were taken from the bulk of a grain and its surface (positions indicated in figure 9(c)), as shown in figure 9(e). No europium is detected in the bulk, whereas the grain boundary contains much Eu and less Al than the bulk AlN. Europium has low solubility in AlN and might form secondary phases at the surface, which is responsible for the 550 nm emission. The existence of such secondary phase was also confirmed by XRD [14]. Thus, the attribution of the 550 nm emission to Eu^{2+} in AlN, based only on emission spectrum, is incorrect. This example illustrates the difficulties in deducing the origin of luminescence peaks [52].

3.3. Strong excitation

The energy of electrons used in CL setup is sufficient to excite almost any luminescence center in the studied material, with the emission spectrum ranging from the ultraviolet to the infrared region [53]. In contrast, the excitation capabilities of photoluminescence (PL) are limited by the incident photon energy [54–56]. As a result, it is easier to study deep UV emission with CL than PL [57–60]. In addition, whereas one incident photon can generate not more than one e–h pair, one incident electron of energy E produces $\sim E/3E_g$ pairs, where E_g is the band gap of the material [3, 4], i.e. orders of magnitude more than one photon.

We have investigated by CL the optical properties of Ca- and Yb-doped α-SiAlON with a composition of $Ca_{0.095}Yb_{0.005}Si_{6.75}Al_{5.25}O_{1.75}N_{14.25}$ [10, 11]. Figure 10(a)

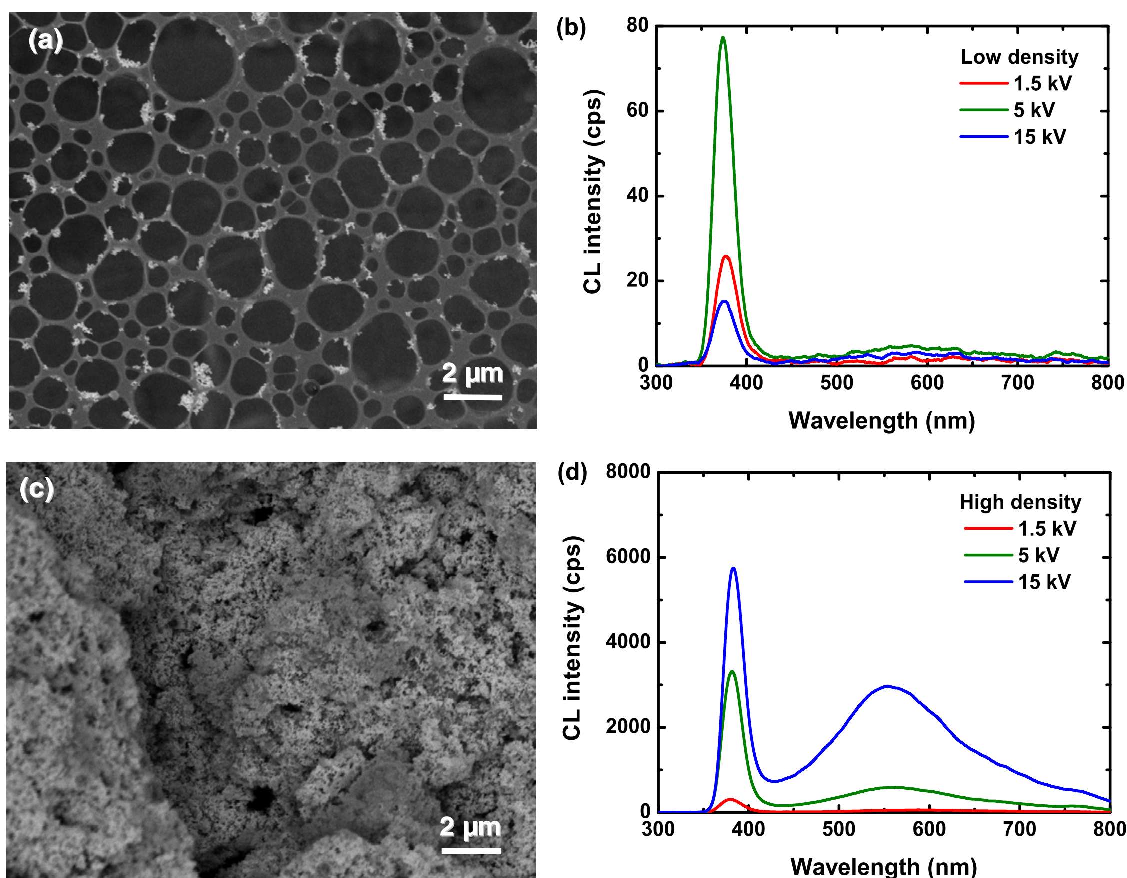

Figure 11. SEM images and CL spectra for low (a, b) and high density (c, d) specimens taken at 1.5, 5 and 15 kV and 1 nA.

shows the CL spectrum of Ca- and Yb-doped α-SiAlON. The CL spectrum shows a broad band in the green region peaking at 557 nm, which is related to the $4f^{13}5d^1 \rightarrow 4f^{14}$ transition of Yb^{2+} [9], but also a broad peak in the UV region (360 nm) and a sharp peak in the IR region (980 nm). The 360 nm emission is attributed to an AlN secondary phase [50] and the 980 nm emission to an inner 4f–4f transition of Yb^{3+} [61]. To clarify the relation between these emissions, CL images were taken at 360 (b), 557 (c) and 980 nm (d). The Yb^{2+} emission (557 nm) is fairly uniformly distributed in the particles except for the brighter particle edges. The luminescence from AlN secondary phase (360 nm) is observed in several large bright patches. This distribution of the AlN phase was confirmed by the electron probe microanalysis [11]. The distribution of Yb^{3+} emission (980 nm) is similar to that of the secondary phase (360 nm), which means that Yb^{3+} and the AlN secondary phase are related. Therefore, CL reveals that Yb is incorporated in both the α-SiAlON and the AlN phases, but with different valence due to the charge balance.

4. Caution on the quantitative analysis of CL results

As shown in the previous section, with CL it is possible to detect luminescence centers and map their spatial distribution that makes CL a useful qualitative technique. Knowing the e–h pair recombination volume, one may also expect to use CL quantitatively [62]. However, caution is required here because the CL intensity depends on the electron beam parameters, internal light absorption, sample damage by the beam and other factors.

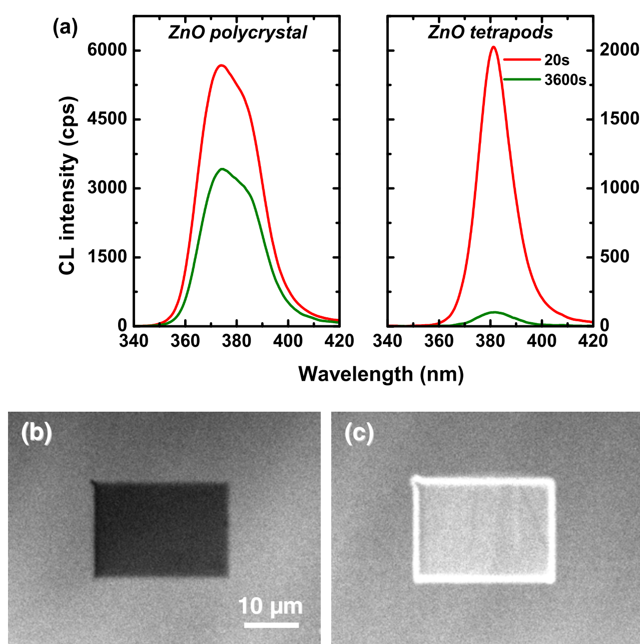

Figure 12. CL spectra of ZnO polycrystal and ZnO tetrapods after 20 and 3600 s of irradiation at 5 kV (a). CL images of an area irradiated at 5 kV for 1 h for O- (a) and Zn-terminated (b) faces of a ZnO single crystal.

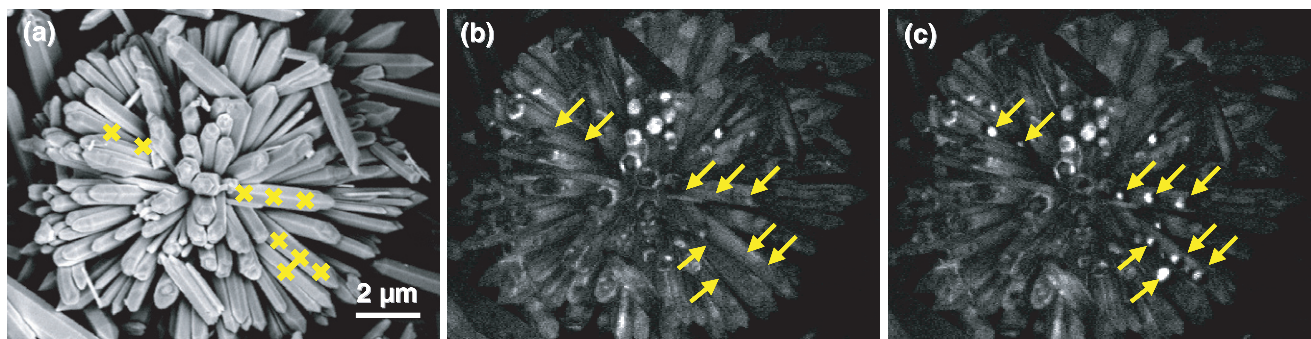

Figure 13. SEM (a) and CL images of the UV emissions before (b) and after (c) 20 s irradiation at 5 kV.

4.1. Measurement conditions

CL results depend not only on the excitation conditions, namely beam current and electron energy, but also on the specimen preparation. Indeed, because CL measurements are rather local, a small variation of these parameters may significantly change the CL intensity.

As an example, we have investigated two samples of the same material having dissimilar concentration of nanoparticles [19]. Different weights of commercial ZnO nanoparticles were dispersed in 5 ml of ethanol to prepare a 'low-density' sample with small segregation and 'high-density' sample with significant agglomeration of particles. Figure 11 shows the SEM images and the CL spectra for low (a, b) and high density (c, d) specimens taken at 1.5, 5 and 15 kV at 1 nA. For the low-density sample, the CL spectrum consists of an excitonic peak at 375 nm; its intensity is the weakest for 15 kV and strongest for the 5 kV excitation. No clear peaks are observed in the visible spectral range. On the contrary, for the high-density sample the UV intensity increases with the electron energy, and the UV peak shifts to the longer wavelength. A clear visible-light peak appears and its intensity increases with the increasing electron energy. The observed change of the UV peak can be related to the generation volume of the e–h pairs. For the low-density sample, the penetration depth of the 5 kV e-beam is comparable to the size of the segregated particles. As the electron energy is increased, the penetration depth exceeds the size of the agglomerated particles and most of the incident electrons pass through the nanoparticles without generating e–h pairs. Thus, the number of generated carriers per nanoparticle and the CL intensity decrease in the low-density sample for the 15 kV excitation. The opposite intensity behavior is observed for the high-density sample because of the larger size of its aggregated particle clusters, and thus a large volume is excited with 15 kV than 5 kV electrons. The saturation of the UV emission and the supralinear increase of visible emission for high-energy electrons in the high-density sample can be explained by the reabsorption of the UV light from the deeper region by the emission centers near the surface [36, 37, 63]. The reabsorbed UV light generates secondary electron–hole pairs and contributes to a new recombination process, which may result in the reemission of UV light or generation of visible light. Thus, a part of UV emission is converted into visible light. The excitonic emission should suffer stronger absorption than the shallow-level emission. This explains the redshift of the UV peak position. Thus, due to the variation of the generation volume and secondary excitation, different CL results can be obtained from the very same nanoparticles dispersed to different densities.

4.2. Variation of the CL intensity during the measurements

Another difficulty in CL observations is the change of the luminescence during the measurements. Relatively high energy of the electron beam increases the chance of sample damage during the CL measurements as compared to PL. This damage can occur via different mechanisms, such as adsorption/desorption or charging at the surfaces, creation or activation of defects, etc [64–71]. Such e-beam induced effects reduce the reliability of quantitative CL measurements.

We have observed a significant degradation of the CL intensity in ZnO [21, 22, 70, 71]. Figure 12(a) shows the CL spectra of a bulk ZnO polycrystal and nanorod-structured ZnO tetrapods, after 20 and 3600 s of irradiation at 5 kV. The UV intensity decreases from 5600 to 3500 counts per second (cps) for ZnO polycrystal and from 2000 to 100 cps for the ZnO tetrapods. This result reveals more serious degradation in nanostructures, which have the higher surface/volume ratio. We have also tested CL stability in ZnO single crystals with (000–1)/O-terminated surface and (0001)/Zn-terminated surfaces [23]. Figures 12(b) and (c) show the respective CL images of the O- and Zn-faces irradiated for 3600 s. The luminescence is weaker in the irradiated than in the unirradiated area for the O-face, but it is stronger for the Zn-face. This experiment suggests that the surface plays an important role in the variation of the intensity during CL measurements [71].

Although these intensity variations complicate the quantitative analysis of CL results, they can be used to investigate the lifetime of optoelectronic devices. Additionally, the e-beam induced effects can be intentionally used to locally alter the luminescence that can be applied to high-density optical data storage or high-resolution UV-emission displays. For such demonstration, we have irradiated some portions of ZnO nanoflowers for 20 s at 5 kV. Figure 13 shows the SEM (a) and CL images of the UV emissions before (b) and after irradiation (c) revealing the

brightening of the UV emission from the parts marked by arrows.

5. Conclusion

We have demonstrated the advantages of CL for luminescence characterization. By revealing the luminescence centers in the material and their spatial distribution, CL can clarify the origin of emission peaks and the growth mechanism. However, the measurement conditions and the e-beam induced degradation must be taken into consideration for quantitative analysis of CL results. When using CL with such caution, it becomes an invaluable technique for the characterization of optoelectronic materials.

Acknowledgments

The authors are grateful to Professor B P Zhang (Xiamen University) for provision of ZnO nanotubes, Dr B D Liu (MANA, NIMS) for $ZnGa_2O_4$ nanorods, Dr C Li (MANA, NIMS) for Zn_2SiO_4 nanotubes, Dr U K Gautam (MANA, NIMS) for ZnO nanoflowers, Dr N Hirosaki and Dr R-J Xie (NIMS) for rare-earth doped oxynitrides, and Dr L Lazzarini and Professor G Salviati (IMEM-CNR Institute) for ZnO tetrapods. The authors also wish to thank Mr Ray Phillips of Julius Kruttschnitt Mineral Research Centre, University of Queensland, Australia, for a discussion and improvement of the manuscript.

References

[1] Gustafssom A, Pistol M E, Montelius L and Samuelson L 1998 *J. Appl. Phys.* **84** 1715
[2] Gustafsson A and Kapon E 1998 *Scanning Microsc.* **12** 285
[3] Yacobi B G and Holt D B 1990 *Cathodoluminescence Microscopy of Inorganic Solids* (New York: Plenum)
[4] Yacobi B G and Holt D B 1985 *J. Appl. Phys.* **59** R1
[5] Kanaya K and Okayama S 1972 *J. Phys D: Appl. Phys.* **5** 43
[6] Toth M and Philips M R 1998 *Scanning* **20** 425
[7] Fonoberov V A and Balandin A A 2004 *Appl. Phys. Lett.* **85** 5971
[8] Soudi A, Dhakal P and Gu Y 2010 *Appl. Phys. Lett.* **96** 253115
[9] Xie R-J, Hirosaki N, Mitomo M, Uheda K, Suehiro T, Xu X, Yamamoto Y and Sekiguchi T 2005 *J. Phys. Chem.* B **109** 9490
[10] Dierre B, Yuan X L, Hirosaki N, Xie R-J and Sekiguchi T 2008 *Mater. Sci. Eng.* B **146** 80
[11] Dierre B, Yuan X L, Hirosaki N, Kimura T, Xie R-J and Sekiguchi T 2008 *J. Mater. Res.* **23** 1701
[12] Hirosaki N, Xie R-J, Inoue K, Sekiguchi T, Dierre B and Tamura K 2007 *Appl. Phys. Lett.* **91** 061101
[13] Inoue K, Hirosaki N, Xie R-J and Takeda T 2009 *J. Phys. Chem.* C **113** 9392
[14] Dierre B, Yuan X L, Inoue K, Hirosaki N, Xie R-J and Sekiguchi T 2009 *J. Am. Ceram. Soc.* **92** 1272
[15] Li C, Bando Y, Dierre B, Sekiguchi T, Huang Y, Lin J and Golberg D 2010 *Nanoscale Res. Lett.* **5** 773
[16] Liu B D, Bando Y, Dierre B, Sekiguchi T, Tang C C, Mitome M, Wu A M, Jiang X and Golberg D 2009 *Nanotechnology* **20** 365705
[17] Yuan X L, Zhang B P, Niitsuma J and Sekiguchi T 2006 *Mater. Sci. Semicond. Proc.* **9** 146
[18] Yuan X L, Dierre B, Wang J B, Zhang B P and Sekiguchi T 2007 *J. Nanosci. Nanotechnol.* **7** 3323
[19] Dierre B, Yuan X L, Ohashi N and Sekiguchi T 2008 *J. Appl. Phys.* **103** 083551
[20] Gautam U K *et al* 2010 Proc. Natl. Acad. Sci. USA doi/10.1073/pnas.1008240107
[21] Lazzarini L, Salviati G, Fabbri F, Zha M Z, Calestani D, Zappettini A, Sekiguchi T and Dierre B 2009 *ACS Nano* **3** 3158
[22] Dierre B, Yuan X L, Yao Y Z, Yokoyama M and Sekiguchi T 2008 *J. Mater. Sci: Mater. Electron.* **19** S307
[23] Dierre B, Yuan X L and Sekiguchi T 2008 *J. Appl. Phys.* **104** 043528
[24] Hidalgo P, Piqueras J, Sochinskii N V, Abellán M, Saucedo E and Diéguez E 2008 *J. Mater. Sci.* **43** 5605
[25] Wei T B, Duan R F, Wang J X, Li J M, Huo Z Q and Zeng Y P 2008 *Microelectron. J.* **39** 1556
[26] Yan J, Fang X S, Zhang L, Bando Y, Gautam U K, Dierre B, Sekiguchi T and Golberg D 2008 *Nano Lett.* **8** 2794
[27] Calleja E, Sánchez-Garcia M A, Sánchez F J, Calle F, Naranjo F B, Muñoz E, Jahn U and Ploog K 2000 *Phys. Rev.* B **62** 16826
[28] Zollfrank C, Rambo C R, Batentschuk M and Greil P 2007 *J. Mater. Sci.* **42** 6325
[29] Jung M N, Ha S Y, Park S H, Yang M, Kim H S, Lee W H, Yao T and Chang J H 2006 *Physica* E **31** 187
[30] Sekiguchi T, Miyashita S, Obara K, Shishido T and Sakagami N 2000 *J. Cryst. Growth* **214/215** 72
[31] Strassburg M *et al* 2004 *Phys. Status Solidi* b **241** 607
[32] Feng X, Yuan X L, Sekiguchi T, Lin W Z and Kang J Y 2005 *J. Phys. Chem.* B **100** 15786
[33] Yu D P, Hang Q L, Ding Y, Zhang H Z, Bai Z G, Wang J J, Zou Y H, Qian W, Xiong G C and Feng S Q 1998 *Appl. Phys. Lett.* **73** 3076
[34] Gautam U K, Panchakarla L S, Dierre B, Fang X S, Bando Y, Sekiguchi T, Govindaraj A, Golberg D and Rao C N R 2009 *Adv. Funct. Mater.* **19** 131
[35] Brillson L J *et al* 2002 *Appl. Surf. Sci.* **190** 498
[36] Brillson L J, Mosbacker H L, Doutt D L, Dong Y, Fang Z Q, Look D C, Cantwell G, Zhang J and Song J J 2009 *Superlattice Microstruct.* **45** 206
[37] Ong H C, Li A S K and Du G T 2001 *Appl. Phys. Lett.* **78** 2667
[38] Kim J S *et al* 2003 *Appl. Phys. Lett.* **82** 2029
[39] Hsieh I J, Chu K T, Yu C F and Feng M S 1994 *J. Appl. Phys.* **76** 3735
[40] Hu J Q, Bando Y and Liu Z W 2003 *Adv. Mater.* **15** 1000
[41] Zhang B P, Manh L H, Wakatsuki K, Ohnishi T, Lippmaa M, Usami N, Kawasaki M and Segawa Y 2003 *Japan. J. Appl. Phys.* **42** 2291
[42] Zhang B P, Binh N T, Segawa Y, Wakatsuki K and Usami N 2003 *Appl. Phys. Lett.* **83** 1635
[43] Sugahara T, Sata H, Hao M S, Naoi Y, Kurai S, Tottori S, Yamashita K, Nishino K, Romano L T and Sakai S 1998 *Japan. J. Appl. Phys.* **37** L398
[44] Thonke K, Schirra M, Schneider R, Reiser A, Prinz G M, Feneberg M, Biskupek J, Kaiser U and Sauer R 2009 *Microelectron. J.* **40** 210
[45] Sekiguchi T and Koizumi S 2002 *Appl. Phys. Lett.* **81** 1987
[46] Mazzer M *et al* 1996 *Mater. Sci. Eng.* B **42** 43
[47] Ewing D J, Porter L M, Wahab Q, Ma X, Sudharshan T S, Tumakha S, Gao M and Brillson L J 2007 *J. Appl. Phys.* **101** 114514
[48] Maximenko S I, Mazeina L, Picard Y N, Freitas J A, Bermudez V M and Prokes S M 2009 *Nano Lett.* **9** 3245
[49] Jaffrennou P, Barjon J, Lauret J-S, Attal-Trétout B, Ducastelle F and Loiseau A 2007 *J. Appl. Phys.* **102** 116102
[50] Slack G A, Schowalter L J, Morelli D and Freitas J A Jr 2002 *J. Cryst. Growth* **246** 287

[51] Hara K, Hikita H, Lai G C and Sakurai T 2004 *Proc. 12th Int. Workshop on Inorganic and Organic Electroluminescence and 2004 Int. Conf. on the Science and Technology of Emissive Displays and Lighting (International Conference Service, Toronto)* p 24

[52] Kawano T, Morito H, Yamada T, Onuma T, Chichibu S F and Yamane H 2009 *J. Solid State Chem.* **182** 2947

[53] Lozykowski H J, Jadwisienczak W M and Brown I 1999 *Appl. Phys. Lett.* **74** 1129

[54] Diaz-Guerra C, Remon A, Garcia J A and Piqueras J 1997 *Phys. Status Solidi* A **163** 497

[55] Jaffrennou P *et al* 2008 *Phys. Rev.* B **77** 235422

[56] Chen S Q, Dierre B, Lee W, Sekiguchi T, Tomita S, Kudo H and Akimoto K 2010 *Appl. Phys. Lett.* **96** 181901

[57] Watanabe K, Taniguchi T and Kanda H 2004 *Phys. Status Solidi* a **11** 2561

[58] Huang Y, Bando Y, Tang C C, Zhi C Y, Terao T, Dierre B, Sekiguchi T and Golberg D 2009 *Nanotechnology* **20** 085705

[59] Watanabe H and Okushi H 2000 *Japan. J. Appl. Phys.* **39** L835

[60] Kipshidze G, Kuryatkov V, Borisov B, Nikishin S, Holtz M, Chu S N G and Temkin H 2002 *Phys. Status Solidi* a **192** 286

[61] Kenyon A J 2002 *Prog. Quantum Electron.* **26** 225

[62] Leto A, Porporati A A, Zhu W L, Green M and Pezzotti G 2007 *J. Appl. Phys.* **101** 093514

[63] Knobloch K, Perlin P, Krueger J, Weber E R and Kisielowski C 1998 *MRS Internet J. Nitride Semicond. Res.* **3** 4

[64] Swart H C, Sebastian J S, Trottier T A, Jones S L and Holloway P H 1996 *J. Vac. Sci. Technol.* A **14** 1697

[65] Zhao Y, Li D S, X S X, Sang W B, Yang D R and Jiang M H 2007 *Solid State Commun.* **143** 197

[66] Fitting H J, Barfels T, Trukhin A N, Scmidt B, Gulans A and von Czarnowski A 2002 *J. Non-Cryst. Solids* **303** 218

[67] Pozina G, Paskov P P, Bergman J P, Hemmingsson C, Hultman L, Monemar B, Amano H, Akasaki I and Usui A 2007 *Appl. Phys. Lett.* **91** 221901

[68] Fabbri F, Cavallini A, Attolini G, Rossi F, Salviati G, Dierre B, Fukata N and Sekiguchi T 2008 *Mater. Sci. Semicon. Proc.* **11** 179

[69] Dong Y F, Fang Z-Q, Look D C, Doutt D R, Hetzer M J and Brillson L J 2009 *J. Vac. Sci. Technol.* B **27** 1710

[70] Dierre B, Yuan X L and Sekiguchi T 2009 *Microelectron. J.* **40** 262

[71] Dierre B, Yuan X L, Armani N, Fabbri F, Salviati G, Ueda K and Sekiguchi T 2010 *J. Electron. Mater.* **29** 761